Space-time correlation of slip and tremor during the 2009 Cascadia slow slip event

Noel M. Bartlow,[1] Shin'ichi Miyazaki,[2] Andrew M. Bradley,[1] and Paul Segall[1]

Received 28 June 2011; revised 24 August 2011; accepted 25 August 2011; published 23 September 2011.

[1] Episodic Tremor and Slip (ETS), involving transient deformations accompanied by emergent, low-frequency tremor occurs in subduction zones around the world. ETS events increase the shear stress on locked megathrusts and may potentially trigger damaging earthquakes. Despite the clear association of tremor and slip the physical relationship between them is unresolved. Tremor appears to result from slip on small asperities on the plate interface due to either creep on the surrounding fault, or stress increases ahead of the propagating slow-slip front. Previous studies of migrating slow slip events have not had sufficient spatial and temporal resolution to differentiate between these two models. To address this, we invert GPS data from the August 2009 ETS event in central Cascadia for the space-time evolution of fault slip-rate. We find a correlation in both space and time between tremor epicenters and the independently determined position of high fault slip-rate. This supports the first hypothesis that tremor asperities are loaded directly by slow slip, rather than by stress increases ahead of the slip front, and provides new insights into the mechanics of ETS. **Citation:** Bartlow, N. M., S. Miyazaki, A. M. Bradley, and P. Segall (2011), Space-time correlation of slip and tremor during the 2009 Cascadia slow slip event, *Geophys. Res. Lett.*, *38*, L18309, doi:10.1029/2011GL048714.

1. Introduction

[2] Episodic tremor and slip (ETS) consists of transient deformations recorded by GPS and other geodetic networks accompanied by non-impulsive, low-frequency seismic signals, termed non-volcanic or tectonic tremor [*Rogers and Dragert*, 2003]. ETS events have been recognized in subduction zones around the world [*Peng and Gomberg*, 2010; *Gomberg and Cascadia 2007 and Beyond Working Group*, 2010; *Beroza and Ide*, 2011], including the Cascadia subduction zone in the Pacific Northwest of the U.S.

[3] ETS events repeat rather periodically with inter-event times that vary with location [*Peng and Gomberg*, 2010]. Cascadia in particular is segmented, with broad northern, central, and southern segments that display different repeat intervals. Cascadia experiences ETS lasting weeks to months, repeating roughly every two years in the central segment [*Brudzinski and Allen*, 2007]. Tectonic tremor is thought to be composed, in whole or in part, by individual low-frequency earthquakes [*Shelly et al.*, 2006, 2007]. Recent studies using wave-form correlation and array methods show that tremor is located on or near the plate interface [*Brown et al.*, 2009; *LaRocca et al.*, 2009]. In northern Cascadia slip and tremor have been observed to migrate along strike at rates of roughly 10 km/day [*Wech et al.*, 2009; *Dragert et al.*, 2004]. In this region cumulative fault slip during an ETS event inferred from inversion of GPS displacements and tremor epicenters appear to be nearly co-located [*Wech et al.*, 2009].

[4] The physical mechanism of tremor has not been established. We consider two hypotheses: (1) Tremor results from locally locked asperities within the slipping region; these are loaded by the surrounding slip and ultimately result in local dynamic rupture (Figure 1a). (2) Tremor results from slip on locked asperities due to shear stress concentrations on the plate interface adjacent to the slipping region (Figure 1b). Hypothesis (2) may be supported by the observation that tremor and slow-slip are spatially offset in the Bungo channel, Japan and the Guerrero gap in Mexico [*Hirose et al.*, 2010; *Kostoglodov et al.*, 2010]. To discriminate between these hypotheses requires resolving the location of the slip front relative to tremor during an ETS event. Hypothesis (1) predicts that tremor locations will be in the area of high slip rate at all times. Hypothesis (2) predicts that tremor locations will occur in front of the area of high slip rate, where the stress increases. The objective of this study is to discriminate between these two hypotheses by time-dependent GPS inversion. We obtain the space-time evolution of slip and slip-rate on the plate interface, and compare these results to tremor epicenters independently located using seismic waveforms [*Wech and Creager*, 2008; *Wech*, 2010].

[5] Previous research in the Nankai trough region of Japan has shown that slip and tremor appear to migrate together [*Hirose and Obara*, 2010; *Obara and Sekine*, 2009; *Obara and Hirose*, 2006]. However, these events had rather limited along-strike extent, so that the relationship between tremor and the slip front is not well resolved. Here we analyze data from the August 2009 Cascadia ETS event, which propagated roughly 330 km along strike, and was well recorded by both GPS and seismic networks. In contrast the 2005 Nankai ETS event analyzed by *Hirose and Obara* [2010] was only ~70 km long, and the slip-rate resolution is insufficient to discriminate between the competing hypotheses shown in Figure 1.

2. Methods

[6] The Pacific Northwest deforms relative to stable North America due in large part to the frictional coupling of the Juan de Fuca and North American plates. Previous studies

[1]Department of Geophysics, Stanford University, Stanford, California, USA.
[2]Department of Geophysics, Graduate School of Science, Kyoto University, Kyoto, Japan.

0094-8276/11/2011GL048714

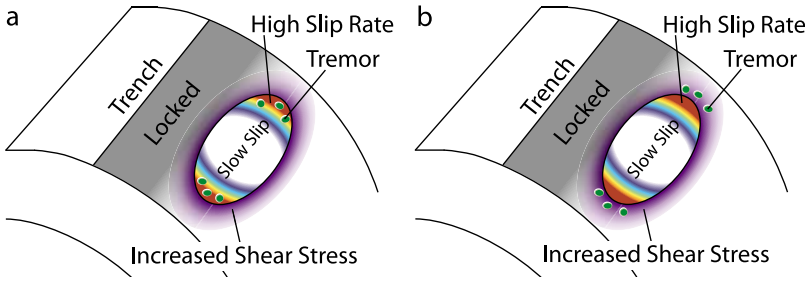

Figure 1. (a, b) Schematic diagrams of two possible relationships between tremor and slow slip.

have shown that average slip-rates during ETS are on the order of 30 cm/year, consistent with our findings of instantaneous slip-rates of 20–150 cm/year [*Wech et al.*, 2009; *Schmidt and Gao*, 2010]. These rates are only an order of magnitude greater than the plate convergence rate (~4 cm/year) [*DeMets et al.*, 2010]. It is therefore important to correct for the secular (inter-ETS) signal. We pre-process the GPS position time series $\boldsymbol{X}(t)$ to remove secular velocities as well as annual and semiannual components using the model equations:

$$\boldsymbol{X}(t) = \boldsymbol{X}(t_0) + \boldsymbol{v}\cdot(t-t_0) + a_1\sin(2\theta) + a_2\cos(2\theta) + s_1\sin(\theta) + s_2\cos(\theta) + Ff(t) + L(\boldsymbol{x}, t-t_0) + \epsilon \quad (1)$$

Here $\boldsymbol{X}(t_0)$ is initial position, $\boldsymbol{v}$ the secular velocity relative to stable North America, $\theta = \pi(t - t_0)/T$ with T equal to one year, F is a Helmert transformation matrix, while $f(t)$ represents the daily frame rotation and translation, L is the local benchmark motion, and ϵ residual error, assumed to be white noise.

[7] We use all available data in the Pacific Northwest plus selected fiducial stations in stable North America, beginning in 2004 for the longest running stations, and estimate the above model terms using a Kalman filter. The frame correction is modeled as white noise. The benchmark motion is modeled as a random walk with scale parameter $\tau = 0.1$ mm/$\sqrt{\text{yr}}$, except during the ETS events where the variance is increased markedly so that data during ETS events do not influence either the secular rates or seasonal terms. We finally subtract only the annual, semi-annual, and secular motions from the time series, leaving the signal of interest in addition to local, reference frame, and other errors.

[8] For the time-dependent fault slip inversion we analyze 50 days of data surrounding the August 2009 ETS event using the Network Inversion Filter (NIF) [*Segall and Matthews*, 1997; *Miyazaki et al.*, 2006]. In this step we include only stations within the Pacific Northwest and estimate only translational corrections to the reference frame. The model equations are now:

$$\boldsymbol{X}(t) = \boldsymbol{X}(t_0) + G\boldsymbol{s}(t-t_0) + Ff(t) + L(\boldsymbol{x}, t-t_0) + \epsilon \quad (2)$$

The second term represents slip on individual fault patches $s(t - t_0)$, multiplying a matrix of elastic Green's functions which give the surface displacement at each GPS station. We employ triangular dislocations in an elastic half-space following *Thomas* [1993] which tessellate the plate interface model of *McCrory et al.* [2004]. Slip on each fault patch has fixed rake angle of 51.7 degrees East of North, chosen to match the convergence direction between the Juan de Fuca and North American plates, calculated from MORVEL at 46°N, −124°E [*DeMets et al.*, 2010]. All other terms are as in equation (1), although τ is set to 1 mm/$\sqrt{\text{yr}}$.

[9] The NIF estimates slip and slip-rate at each daily epoch. Slip-rate is assumed to follow a random walk with scale parameter α, such that slip is an integrated random walk [*Segall and Matthews*, 1997]. Spatial smoothing is implemented via pseudo-observations as by *Segall et al.* [2000]. Spatial and temporal smoothing hyperparameters are chosen by a combination of maximum likelihood following *Segall and Matthews* [1997] and examination of time series fits.

[10] We apply a non-negativity constraint on slip rate using the method of *Simon and Simon* [2006]. At each epoch the Kalman filter estimates the unconstrained slip-rate. The constrained estimate is then the non-negative minimizer of the covariance-weighted L2 norm of the difference between the constrained and unconstrained slip-rates. We solve this bound-constrained convex quadratic program using the software package PDCO (M. A. Saunders, PDCO, Matlab software for convex optimization, 2010, available at http://www.stanford.edu/group/SOL/software/pdco.html). A monotonicity constraint on slip falls outside the statistical framework of *Simon and Simon* [2006]; numerical experiments show that such a constraint systematically over predicts observed displacements and therefore is not applied.

[11] The Network Inversion Filter employs two smoothing hyperparameters, α for temporal smoothing and γ for spatial smoothing (lower values indicate more smoothing). Contouring the likelihood as a function of the hyperparameters with the unconstrained filter, following *Segall and Matthews* [1997], reveals a strong negative correlation between α and γ, with high likelihood ranging from (α = 479, $\gamma = 3.2 \times 10^{-3}$) to ($\alpha = 30.2$, $\gamma = 25.1 \times 10^{-3}$). The estimated slip-rate is insensitive to small (factors of 5) changes in α and γ. Solutions with $\alpha > 200$ are clearly fitting noise in the GPS data (Figure S1 in the auxiliary material).[1] Values near $\alpha \simeq 60$ and $\gamma \simeq 15 \times 10^{-3}$ provide estimates with high likelihood and reasonable fits to the time series (Figure 2).

3. Results

[12] The final slip distribution for the August 2009 ETS event is shown in Figure 3. Slip is concentrated from 35 km

[1] Auxiliary materials are available in the HTML. doi:10.1029/2011GL048714.

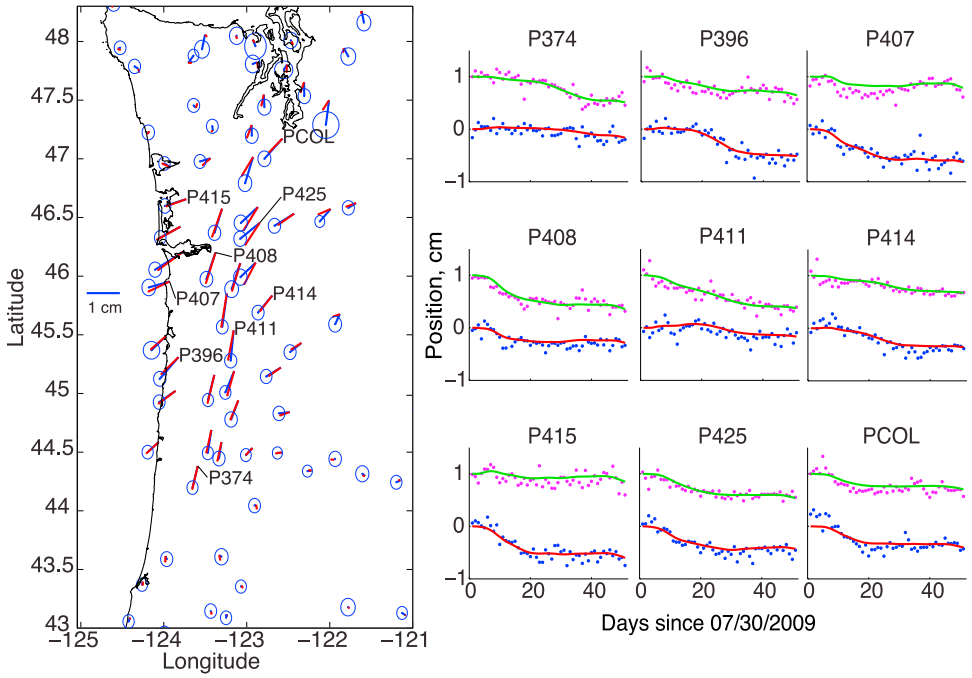

Figure 2. (left) Observed and predicted cumulative GPS displacements during the 2009 ETS event. Data and 1σ error ellipses shown in blue; model fit shown in red. Labeled stations refer to time series fits shown to the right. (right) Time series fits to GPS data for selected stations. Blue dots represent east displacements with model fit in red continuous line; pink dots represents north displacements with model fit in green. North component offset by 1 cm for clarity.

to 50 km depth, with maximum slip between 4–5 cm. There is some negative slip, which is completely below the formal 1 sigma error level of ~2 cm, and is therefore indistinguishable from zero. While a non-negativity constraint was applied to slip-rate, slip is adjusted in the filter to fit the GPS data and therefore can be negative. The cumulative moment is 1.65×10^{19} N-m, assuming a shear modulus of 3×10^{10} Pa, equivalent to a moment magnitude of 6.8. The surface projection of slip and tremor epicenters are generally very well correlated, although slip in the northern section is

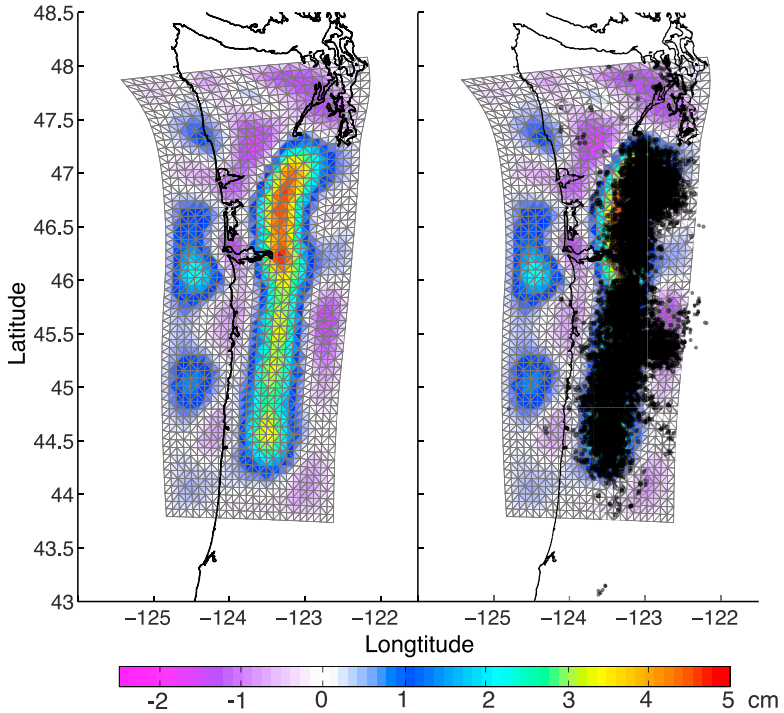

Figure 3. Estimated cumulative slip on the plate interface for the August 2009 ETS event. (left) Slip at final epoch. (right) Same as Figure 3 (left) but with tremor epicenters for the time interval 08/02/2009–09/22/2009 plotted in black.

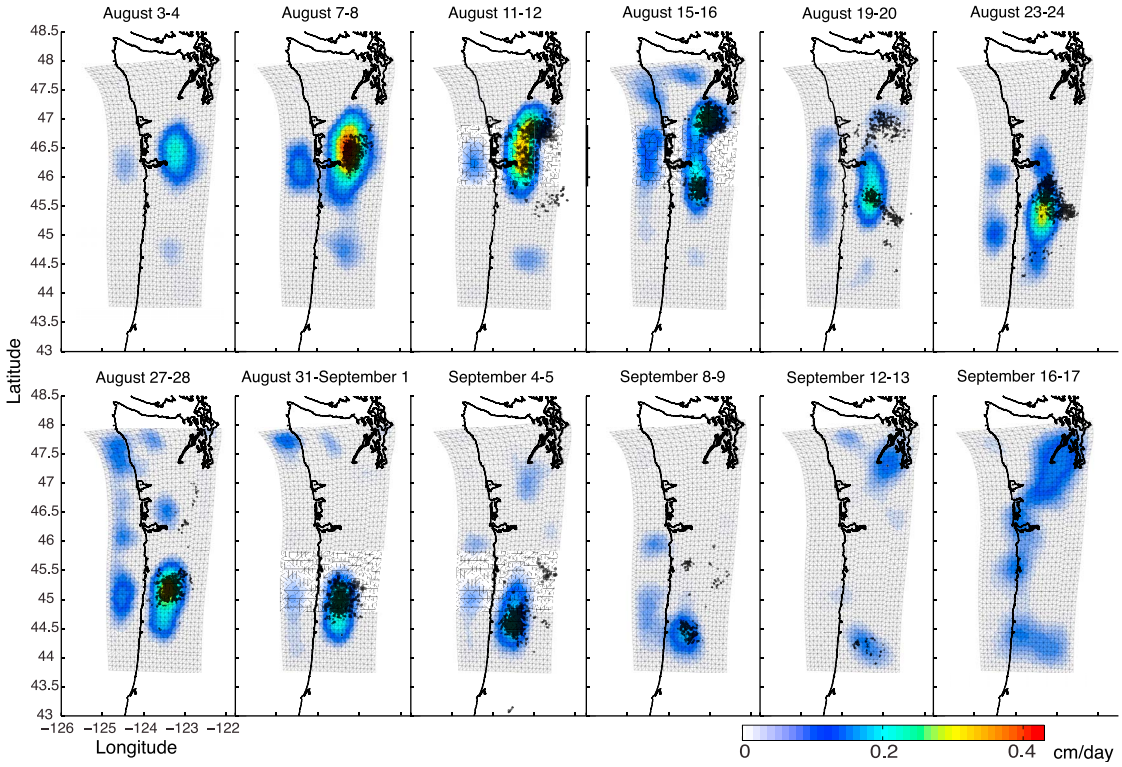

Figure 4. Slip rate on the plate interface, averaged over two day intervals. Tremor epicenters are plotted in black for the same two-day intervals. The plate interface mesh is shown between 10 and 60 km depth. Note that not all of the modeled days are shown.

slightly shallower than the tremor. There are also two tremor clusters near 47°N and 45.5°N latitude that appear deeper than any resolved slip. Fits to the GPS data in both space and time are generally good (Figure 2).

[13] Snapshots of slip-rate and tremor averaged over two day intervals are shown in Figure 4. Tremor starts near 46.5°N on 6 August 2009 and propagates both north and south. By 15 August tremor has split into two groups; the northern cloud disappears soon after, while the southern cloud continues to propagate south. Inversion of the GPS data resolves a similar splitting and migration of the slipping region (Figure 4). We find an excellent correlation between the instantaneous region of high slip rate and tremor epicenters for all times during the ETS event (Figure 4). This correlation is especially remarkable given that tremor epicenters and slip are obtained from completely independent data.

[14] The slip-rate estimates in Figure 4 are "smoothed" [*Segall and Matthews*, 1997], that is conditional on all data epochs (sometimes referred to as "back-smoothed" in the Kalman filter). This temporal smoothing is known to lead to acausal slip that appears before the true onset of slip, as in the first panel of Figure 4. If tremor events are indeed located within the actively slipping zone, some slip must precede tremor, although given the noise level in the GPS measurements this may be difficult to detect. To more precisely determine the relative onset of tremor and slip we examine "filtered" estimates, that are conditional only on data up to the current epoch (forward filter only). These are generally noisier than the smoothed estimates but causal and therefore more accurate for determining the onset of transient slip [*Murray and Segall*, 2005]. A comparison of the smoothed and filtered estimates of slip-rate starting 2 days before the onset of tremor and ending 3 days after are shown in Figure S2. A small number of tremor events are located on 6 August. By 7 August, the ETS event has clearly begun, with a significant burst of tremor. Similarly, by 7 August the filtered slip-rate estimates have resolved significant slip in the same location, demonstrating that tremor and slip started within one day of one another. It is likely that some slip occurred on 6 August, however the GPS data cannot resolve this. *Gomberg and Cascadia 2007 and Beyond Working Group* [2010] show that tremor and slip in Cascadia have onsets within ~2 hours, consistent with our "filtered" estimates.

[15] To test the resolution of the inversion we construct synthetic data from an elliptical slip distribution with peak slip of 4 cm. The semi-minor (East-West) axis is fixed, while the semi-major axis grows linearly with time. The estimated and true slip rate histories are shown in Figure 5. White noise is added to match the uncertainty levels in the actual data, with amplitudes of approximately 1.5 mm in the horizontal and 6.5 mm in the vertical. The inversion employs the same hyperparameters ($\alpha = 60$, $\gamma = 15 \times 10^{-3}$) as in the inversion of the actual data. While the estimated slip-rate is significantly smoothed relative to the actual distribution, with some smearing in front of the crack tip, the peak slip rate is always behind the true crack tip by a few tens of kilometers. Figure 4 shows that tremor is generally co-located with the area of high slip-rate, which demonstrates that tremor actually occurs behind the slip front. An exception to this pattern occurs around latitude 45.5, where

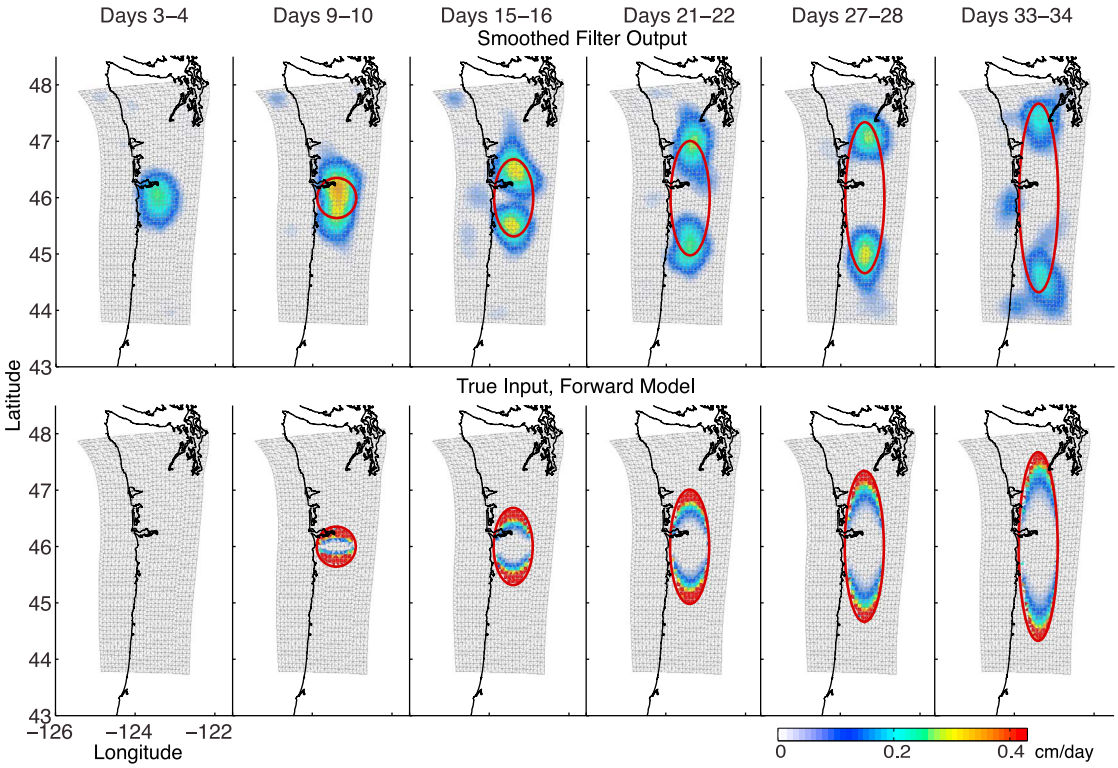

Figure 5. Selected snapshots from the slip-rate history of the resolution test. (top) Smoothed filter result. (bottom) True input distribution from forward model. Red ellipses mark the current position of the slip front. Peak slip rate is resolved behind the slip front.

a cloud of tremor appears downdip from the main area of slip. Tremor actually occurs in the area three times during the migration, appearing as sudden jumps away from the main migration (Animation S1). This may be due to errors in the seismic catalog due to noise or malfunctioning stations. Additionally, in the northern part of the slipping region, tremor appears to be offset from slip slightly in the down-slip direction (Figure 3). Such an offset may be due to inaccurate Green's functions calculations, due to either inaccuracies in the plate interface model, or due to the assumption of a homogenous elastic halfspace.

[16] Our results allow us to reject the hypothesis shown schematically in Figure 1b. The tremor epicenters have location errors of approximately 5–10 kilometers [*Wech and Creager*, 2008], significantly less than the dimension of the tremor cloud in any two day interval. The observed spread of the tremor is thus likely real, although on shorter time scales the tremor appears to be more localized along strike, advancing largely in streaks in the dip-direction [*Ghosh et al.*, 2010].

4. Conclusions

[17] For the August 2009 central Cascadia ETS event, tremor and the area of high slip rate migrate together. The area of high slip rate is shown by inversion of synthetic data to be behind the slip front; therefore tremor is originating from the region behind the crack front as in Figure 1a. We conclude that our findings support the hypothesis that tremor results from local heterogeneities within the slipping region that accelerate to high enough slip speed to radiate seismic waves. This suggests a model in which small steady-state velocity weakening asperities within the slow slip region remain locked as the region begins to slip. These patches are stressed by slip on the surrounding fault, ultimately leading to accelerating slip and inertial instability. Many of these patches within the slow slip region together apparently make up the observed tremor signal.

[18] Our results imply that tremor epicenters may be used as a proxy for the actively slipping region in central Cascadia, and support the interpretation that inter-ETS tremor [*Wech and Creager*, 2008] indeed represents slip below the GPS detection threshold. Furthermore, tremor can be located in near real time during an event, whereas inversions of GPS data have, to date, only been conducted after the fact. If ETS events can trigger or evolve into dynamic megathrust earthquakes, locating active slip via the tremor may prove to be a powerful method for monitoring subduction zone activity.

[19] Further work is needed to confirm the spatial and temporal correlation for other ETS events in Cascadia, and in other well-instrumented subduction zones. In particular, the relationship between tremor and slow slip in regions where there is a significant depth offset between tremor and slip, such as the Bungo channel, Japan and the Guerrero gap in Mexico [*Hirose et al.*, 2010; *Kostoglodov et al.*, 2010], warrants further investigation.

[20] **Acknowledgments.** We thank Aaron Wech and Kenneth Creager for helpful discussions concerning the tremor location method, Yo Fukushima for help with meshing, and two anonymous reviewers for their helpful comments. Funding provided by grants NSF EAR-0838267 and NEHRP G10AP00009. Noel Bartlow is supported by a Gabilan Stanford Graduate Fellowship and a National Science Foundation Graduate Research Fellow-

ship. GPS data used in this paper can be found at the PBO archive hosted by UNAVCO, http://pbo.unavco.org/. Tremor catalog data used in this paper is archived by the Pacific Northwest Seismic Network and can be found at http://www.pnsn.org/tremor/.

References

Beroza, G. C., and S. Ide (2011), Slow earthquakes and nonvolcanic tremor, *Annu. Rev. Earth Planet. Sci.*, *39*, 271–296.

Brown, J. R., G. C. Beroza, S. Ide, K. Ohta, D. R. Shelly, S. Y. Schwartz, W. Rabbel, M. Thorwart, and H. Kao (2009), Deep low-frequency earthquakes in tremor localize to the plate interface in multiple subduction zones, *Geophys. Res. Lett.*, *36*, L19306, doi:10.1029/2009GL040027.

Brudzinski, M. R., and R. M. Allen (2007), Segmentation in episodic tremor and slip all along Cascadia, *Geology*, *35*, 907–910, doi:10.1130/G23740A.1.

DeMets, C., R. G. Gordon, and D. F. Argus (2010), Geologically current plate motions, *Geophys. J. Int.*, *181*, 1–80, doi:10.1111/j.1365-246X.2009.04491.x.

Dragert, H., K. Wang, and G. Rogers (2004), Geodetic and seismic signatures of episodic tremor and slip in the northern Cascadia subduction zone, *Earth Planets Space*, *56*, 1143–1150.

Ghosh, A., J. E. Vidale, J. R. Sweet, K. C. Creager, A. G. Wech, H. Houston, and E. E. Brodsky (2010), Rapid, continuous streaking of tremor in Cascadia, *Geochem. Geophys. Geosyst.*, *11*, Q12010, doi:10.1029/2010GC003305.

Gomberg, J., and Cascadia 2007 and Beyond Working Group (2010), Slow-slip phenomena in Cascadia from 2007 and beyond: A review, *Geol. Soc. Am. Bull.*, *112*, 963–978, doi:10.1130/B30287.1.

Hirose, H., and K. Obara (2010), Recurrence behavior of short-term slow slip and correlated nonvolcanic tremor episodes in western Shikoku, southwest Japan, *J. Geophys. Res.*, *115*, B00A21, doi:10.1029/2008JB006050.

Hirose, H., Y. Asano, K. Obara, T. Kimura, T. Matsuzawa, S. Tanaka, and T. Maeda (2010), Slow earthquakes linked along dip in the Nankai subduction zone, *Science*, *330*, 1502, doi:10.1126/science.1197102.

Kostoglodov, V., A. Husker, N. M. Shapiro, J. S. Payero, M. Campillo, N. Cotte, and R. Clayton (2010), The 2006 slow slip event and nonvolcanic tremor in the Mexican subduction zone, *Geophys. Res. Lett.*, *37*, L24301, doi:10.1029/2010GL045424.

LaRocca, M., K. C. Creager, D Gallusso, S. Malone, J. E. Vidale, J. R. Sweet, and A. G. Wech (2009), Cascadia tremor located near plate interface constrained by *S* minus *P* wave times, *Science*, *323*, 620–623, doi:10.1126/science.1167112.

McCrory, P.A., J. L. Blair, G. H. Oppenheimer, and S. R. Walter (2004), Depth to the Juan de Fuca slab beneath the Cascadia subduction margin: A 3-D model for sorting earthquakes, *U.S. Geol. Surv. Digital Data Ser.*, 91.

Miyazaki, S., P. Segall, J. J. McGuire, T. Kato, and Y. Hatanaka (2006), Spatial and temporal evolution of stress and slip rate during the 2000 Tokai slow earthquake, *J. Geophys. Res.*, *111*, B03409, doi:10.1029/2004JB003426.

Murray, J. R., and P. Segall (2005), Spatiotemporal evolution of a transient slip event on the San Andreas fault near Parkfield, California, *J. Geophys. Res.*, *110*, B09407, doi:10.1029/2005JB003651.

Obara, K., and H. Hirose (2006), Non-volcanic deep low-frequency tremors accompanying slow slips in the southwest Japan subduction zone, *Tectonophysics*, *417*, 33–51, doi:10.1016/j.tecto.2005.04.013.

Obara, K., and S. Sekine (2009), Characteristic activity and migration of episodic tremor and slow-slip events in central Japan, *Earth Planets Space*, *61*, 853–862.

Peng, Z., and J. Gomberg (2010), An integrated perspective of the continuum between earthquakes and slow-slip phenomena, *Nat. Geosci.*, *3*, 399–607, doi:10.1038/ngeo940.

Rogers, G., and H. Dragert (2003), Episodic tremor and slip on the Cascadia subduction zone: The chatter of slient slip, *Science*, *300*, 1942–1943, doi:10.1126/science.1084783.

Schmidt, D. A., and H. Gao (2010), Source parameters and time-dependent slip distributions of slow slip events on the Cascadia subduction zone from 1998 to 2008, *J. Geophys. Res.*, *115*, B00A18, doi:10.1029/2008JB006045.

Segall, P., and M. Matthews (1997), Time dependent inversion of geodetic data, *J. Geophys. Res.*, *102*, 22,391–22,409.

Segall, P., R. Bürgmann, and M. Matthews (2000), Time-dependent triggered afterslip following the 1989 Loma Prieta earthquake, *J. Geophys. Res.*, *105*, 5615–5634.

Shelly, D. R., G. C. Beroza, S. Ide, and S. Nakamula (2006), Low-frequency earthquakes in Shikoku, Japan, and their relationship to episodic tremor and slip. *Nature*, *442*, 188–191, doi:10.1038/nature04931.

Shelly, D. R., G. C. Beroza, and S. Ide (2007), Non-volanic tremor and low-frequency earthquake swarms, *Nature*, *446*, 305–307, doi:10.1038/nature05666.

Simon, D., and D. L. Simon (2006), Kalman filtering with inequality constraints for turbofan engine health estimation, *IEE Proc. Control Theory Appl.*, *153*, 371–378.

Thomas, A. L. (1993), Poly3D: A three-dimensional, polygonal element, displacement discontinuity boundary element computer program with applications to fractures, faults, and cavities in the Earth's crust, M.S. thesis, Dep. of Geol. and Environ. Sci., Stanford Univ., Stanford, Calif.

Wech, A. G. (2010), Interactive tremor monitoring, *Seismol. Res. Lett.*, *84*, 664–669, doi:10.1785/gssrl.81.4.664.

Wech, A. G., and K. C. Creager (2008), Automated detection and location of Cascadia tremor, *Geophys. Res. Lett.*, *35*, L20302, doi:10.1029/2008GL035458.

Wech, A. G., K. C. Creager, and T. I. Melbourne (2009), Seismic and geodetic constraints on Cascadia slow slip, *J. Geophys. Res.*, *114*, B10316, doi:10.1029/2008JB006090.

N. M. Bartlow, A. M. Bradley, and P. Segall, Department of Geophysics, Stanford University, Mitchell Building, 397 Panama Mall, Stanford, CA 94305, USA. (noelb@stanford.edu)

S. Miyazaki, Department of Geophysics, Graduate School of Science, Kyoto University, Kitashirakawaoiwake-cho, Sakyo-ku, Kyoto-shi, Kyoto 606-8502, Japan.